

SUPPORTING INFORMATION

Electrically Polarized Hydroxyapatite: Influence of the Polarization Process on the Microstructure and Properties

Jordi Sans,^{1,2} Jordi Llorca,^{1,2,3} Vanesa Sanz,⁴ Jordi Puiggali,^{1,2,5}

Pau Turon,^{4,} and Carlos Alemán^{1,2,5,*}*

¹ Departament d'Enginyeria Química, EEBE, Universitat Politècnica de Catalunya, C/ Eduard Maristany, 10-14, Ed. I2, 08019, Barcelona, Spain

² Barcelona Research Center in Multiscale Science and Engineering, Universitat Politècnica de Catalunya, C/ Eduard Maristany, 10-14, 08019, Barcelona, Spain

³ Institut de Tècniques Energètiques, EEBE, Universitat Politècnica de Catalunya, C/ Eduard Maristany, 10-14, Ed. C3, 08019, Barcelona, Spain

⁴ B. Braun Surgical, S.A. Carretera de Terrasa 121, 08191 Rubí (Barcelona), Spain

⁵ Institute for Bioengineering of Catalonia (IBEC), The Barcelona Institute of Science and Technology, Baldiri Reixac 10-12, 08028 Barcelona Spain

Page S2	Complementary description of the synthetic and polarization methods.
Page S5	Table S1. Atomic percent composition (C, O, P and Ca) of HAp(a) and PP/HAp(a) surfaces as determined by XPS.
Page S6.	Figure S1. XRD spectrum of HAp(a) samples showing the presence of β -TCP phase.
Page S7	Figure S2. XRD spectrum of HAp(w) samples showing the presence of β -TCP phase.
Page S8.	Figure S3. Raman spectra of HAp(a) and PP/HAp(a) samples.
Page S9	Figure S4. Yield of the polarization treatment as a function

	of temperature. Figure S5. Yield of the polarization treatment at 1000 °C as a function of the cooling rate.
Page S10	Figure S6. Evolution of the content of ACP and β -TCP crystalline phases as a function of the depth determined by Raman spectroscopy for PP/HAp(a) and SP1/HAp(w).
Page S11	Figure S7. High magnification SEM micrograph of HAp(w).
Page S12	Figure S8. High magnification SEM micrograph of PP/HAp(a) and SP1/HAp(w).
Page S13	Figure S9. TEM image of PP/HAp(a) showing the sintering of the particles.

METHODS

Hydrothermal synthesis of hydroxyapatite (HAp)

15 mL of 0.5 M of $(\text{NH}_4)_2\text{HPO}_4$ in de-ionized water were added at a rate of 2 mL \cdot min⁻¹ to 25 mL of 0.5 M of $\text{Ca}(\text{NO}_3)_2$ in ethanol (with pH previously adjusted to 10.5 using ammonium hydroxide solution) and left aging for 1 h. The whole process was performed under gentle agitation (150 rpm) and at room temperature. Hydrothermal treatment at 150 °C was applied using an autoclave Digestec DAB – 2 for 24h. The autoclave is allowed to cool down before opening. The precipitates were separated by centrifugation and washed with water and a 60/40 v/v mixture of ethanol – water (twice). Then, samples were freeze–drying for 3 days. For this purpose, samples were left for 3 h in the freezer at -87 °C and, subsequently, the freeze-drying was performed using a TelStar LyoQuest pre-cooled at -53.7 °C. The working pressure during the freeze–drying process was 0.089 mbar, while the temperature was kept at -53.7 °C, respectively. After complete the freeze-drying, the white powder obtained was sintered for 2 h at 1000 °C in air and vapor atmospheres using the Carbolite ELF11/6B/301 furnace.

Polarization of HAp by using thermal stimulation

Mechanical consistent discs of ~1.5 mm of thickness were obtained by pressing 150 mg of cHAp powder at 620 MPa for 10 min using a manual hydraulic press SPECAC. Thermal polarization was done placing the cHAp discs between two stainless steel (AISI 304) and applying a desired constant DC voltage for 1 h using the a GAMMA power supply at different temperatures using the same laboratory furnace. The discs were allowed to cool down

maintaining the applied electric potential for 30 minutes, and finally, all the system was powered off and left to cool overnight.

X-ray photoelectron spectroscopy (XPS)

XPS analyses were performed in a SPECS system equipped with a high-intensity twin-anode X-ray source XR50 of Mg/Al (1253 eV/1487 eV) operating at 150 W, placed perpendicular to the analyzer axis, and using a Phoibos 150 MCD-9 XP detector. The X-ray spot size was 650 μm . The pass energy was set to 25 and 0.1 eV for the survey and the narrow scans, respectively. Charge compensation was achieved with a combination of electron and argon ion flood guns. The energy and emission current of the electrons were 4 eV and 0.35 mA, respectively. For the argon gun, the energy and the emission current were 0 eV and 0.1 mA, respectively. The spectra were recorded with pass energy of 25 eV in 0.1 eV steps at a pressure below 6×10^{-9} mbar. These standard conditions of charge compensation resulted in a negative but perfectly uniform static charge. The C 1s peak was used as an internal reference with a binding energy of 284.8 eV. The surface composition was determined using the manufacturer's sensitivity factors.

Table S1. Atomic percent composition (C, O, P and Ca) of HAp(a) and PP/HAp(a) surfaces as determined by XPS.

Sample	%Atomic Concentration			
	C ^(a)	O ^(a)	P	Ca
HAp(a)	14.37	43.06	18.51	24.07
PP-HAp	15.13	40.96	17.79	26.13

^(a) The content of C and O is influenced by CO₂ contamination, as usual.

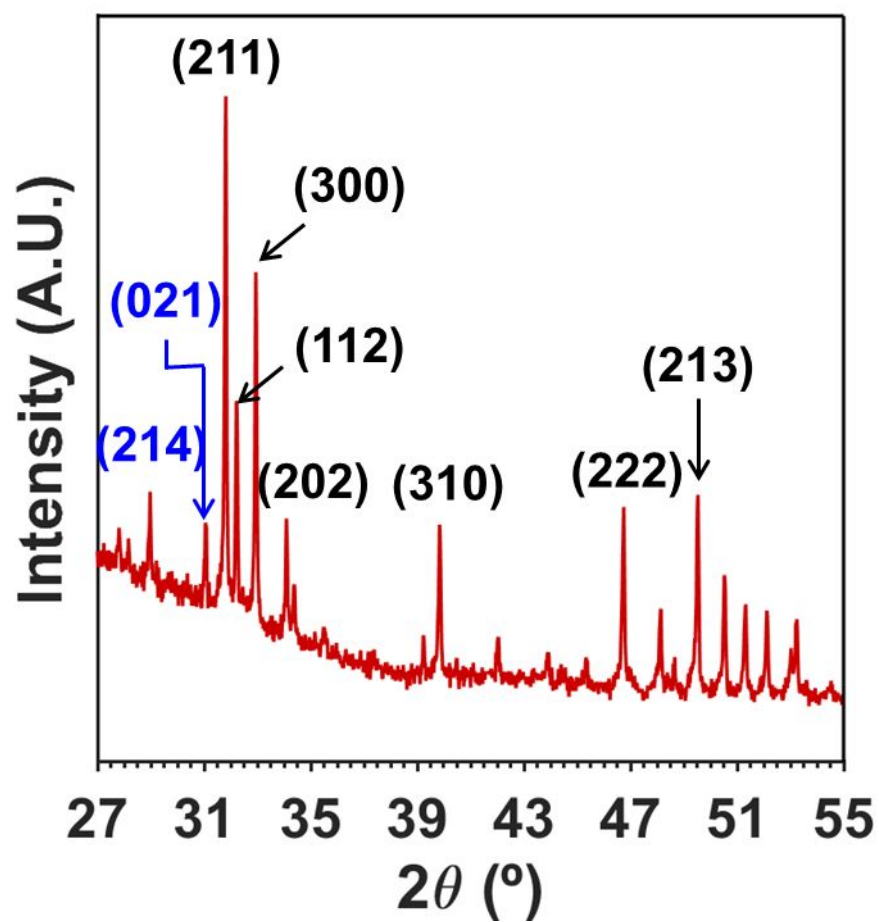


Figure S1. XRD spectrum of HAp(a) samples showing the presence of β -TCP phase. Characteristic reflections of HAp and β -TCP are displayed in black and blue, respectively

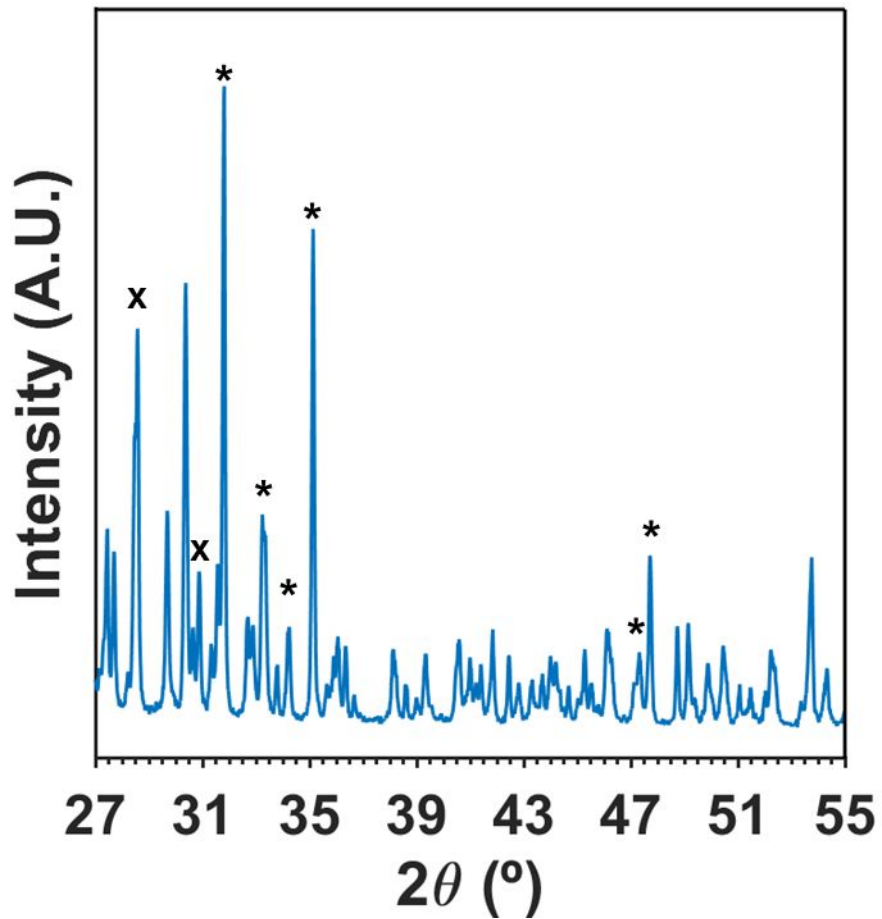


Figure S2. XRD spectrum of HAp(w) samples showing the presence of β -TCP phase. Characteristic reflections of HAp and β -TCP are displayed in asterisks and crosses, respectively. The high scattering and splitting, which are associated to distortions in phase transformations, make difficult the assignation of many signals

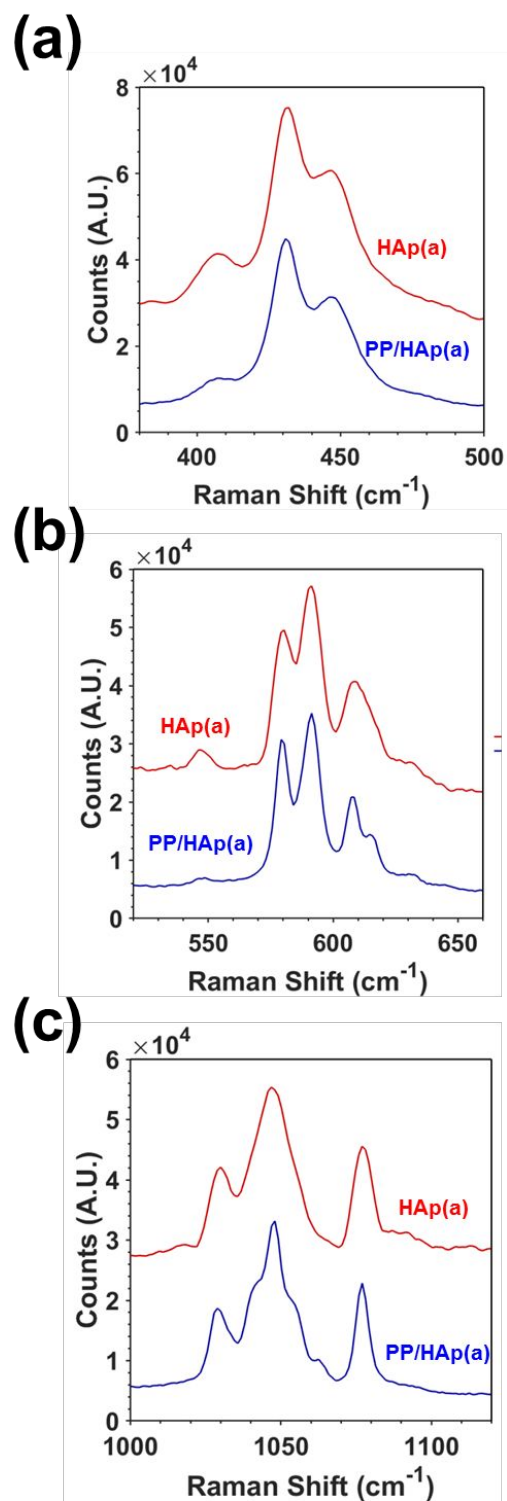


Figure S3. Raman spectra of HAp(a) and PP/HAp(a) samples showing the different vibrational modes located at (a) $\nu_2 = 400\text{-}900 \text{ cm}^{-1}$; (b) $\nu_3 = 570\text{-}625 \text{ cm}^{-1}$; (c) $\nu_4 = 1020\text{-}1095 \text{ cm}^{-1}$.

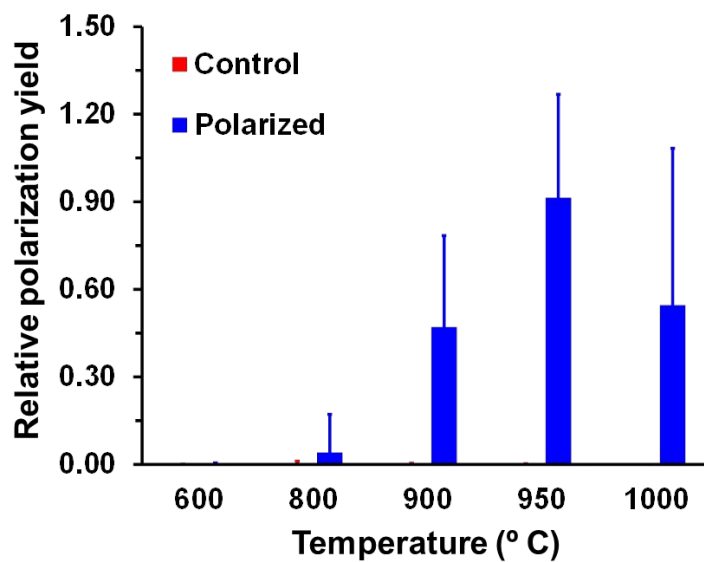


Figure S4. Yield of the polarization treatment as a function of temperature.

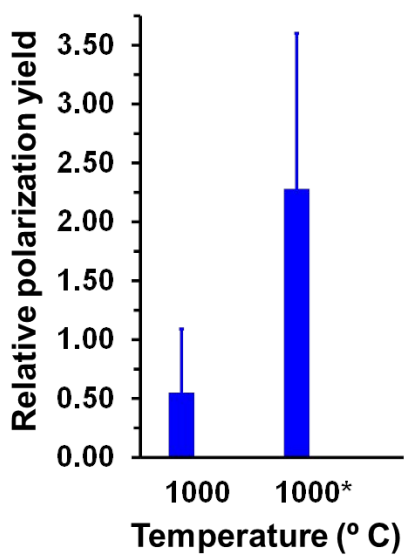


Figure S5. Yield of the polarization treatment at 1000 °C as a function of the cooling rate (* refers to fast cooling down).

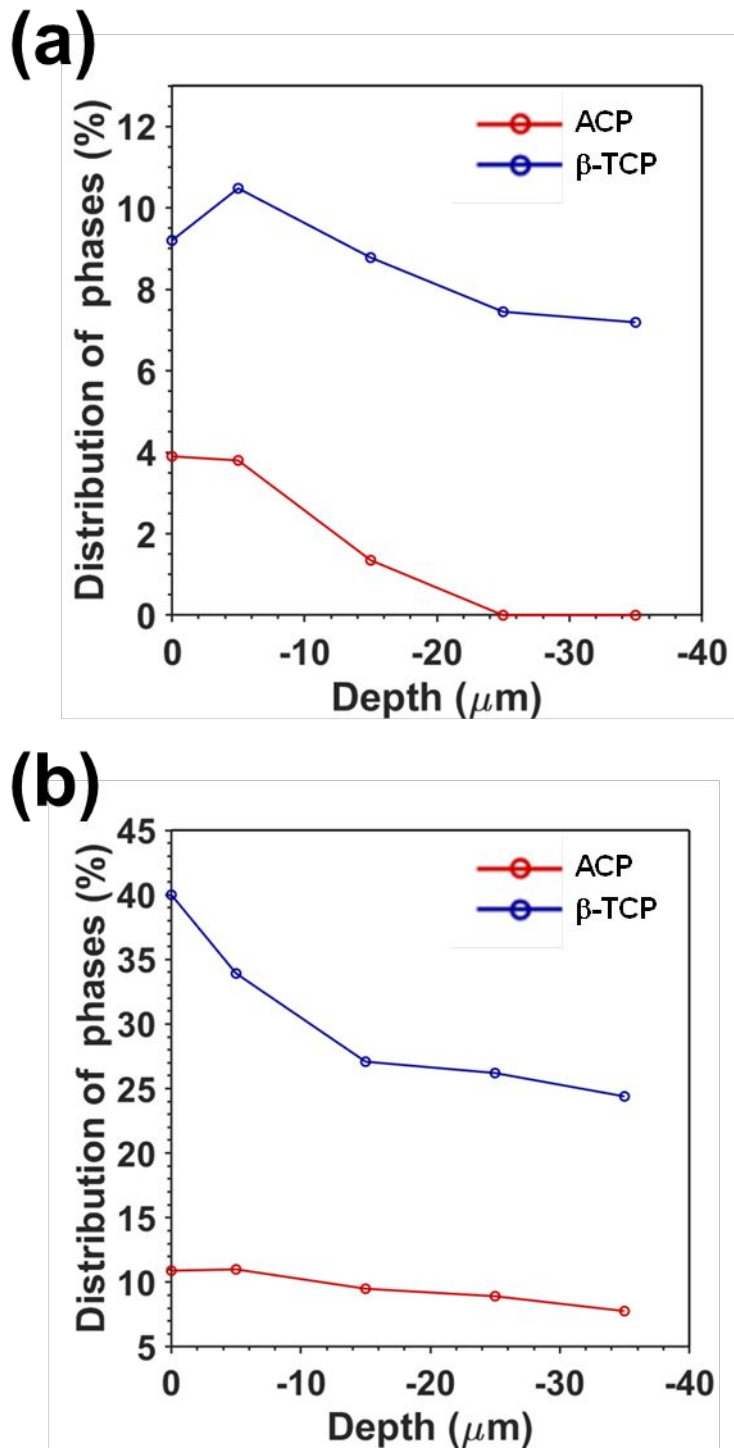


Figure S6. Evolution of the content of ACP and β -TCP crystalline phases as a function of the depth determined by Raman spectroscopy for (a) PP/HAp(a) and (b) SP1/HAp(w).

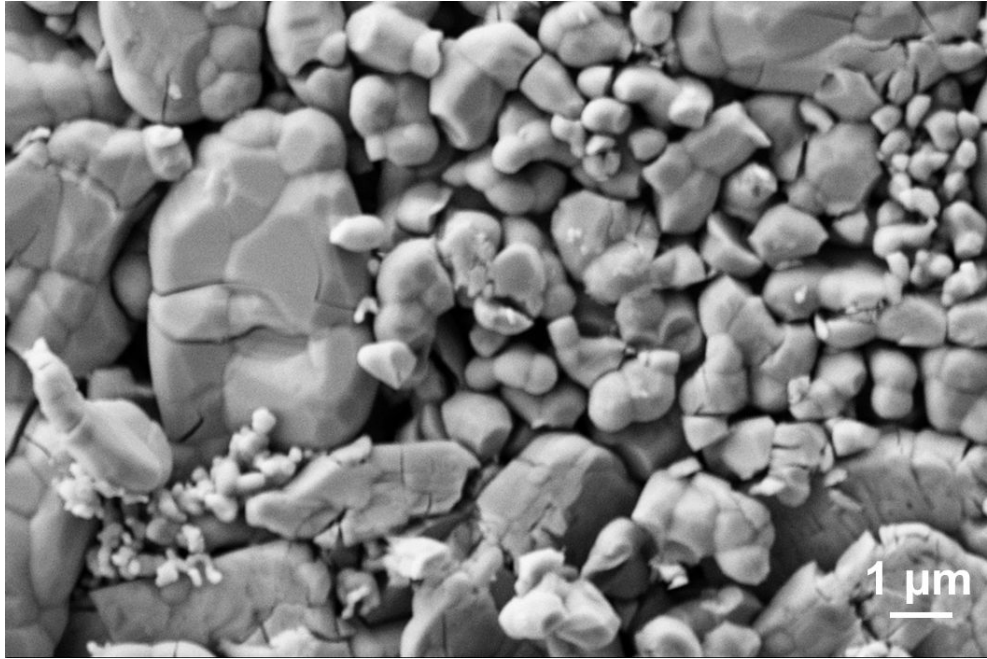


Figure S7. High magnification SEM micrograph of HAp(w).

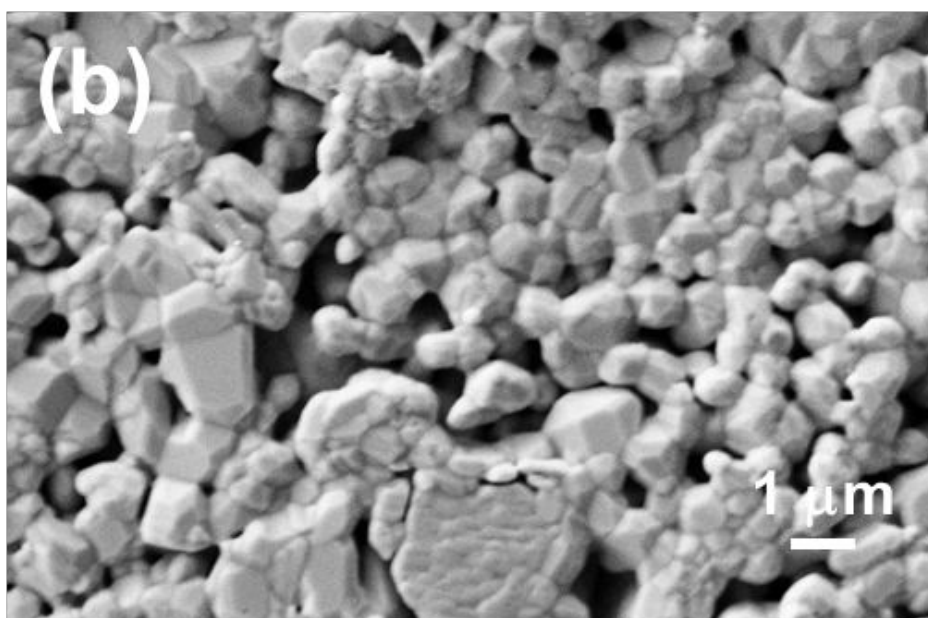
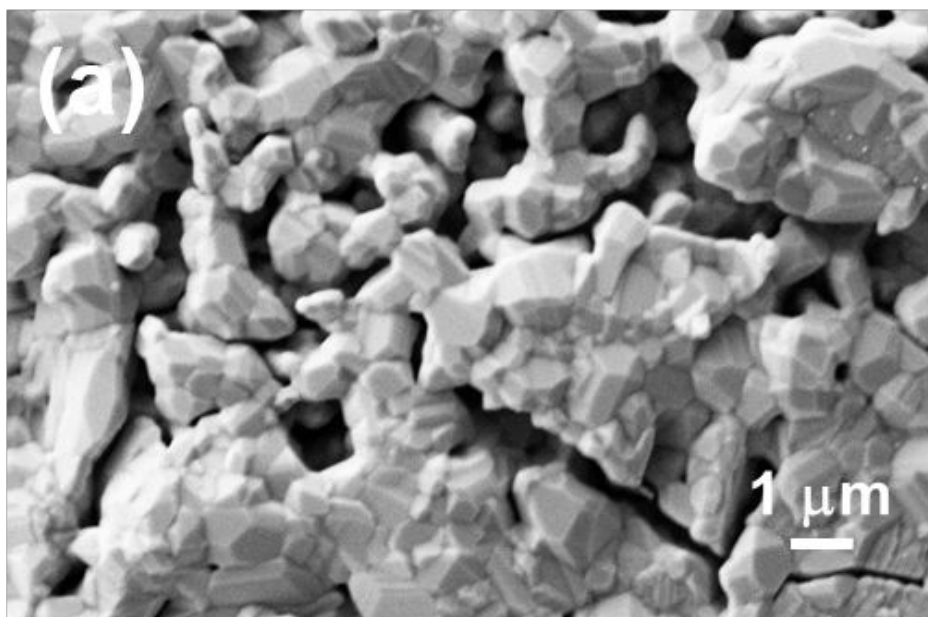


Figure S8. High magnification SEM micrograph of (a) PP/HAp(a) and (b) SP1/HAp(w).

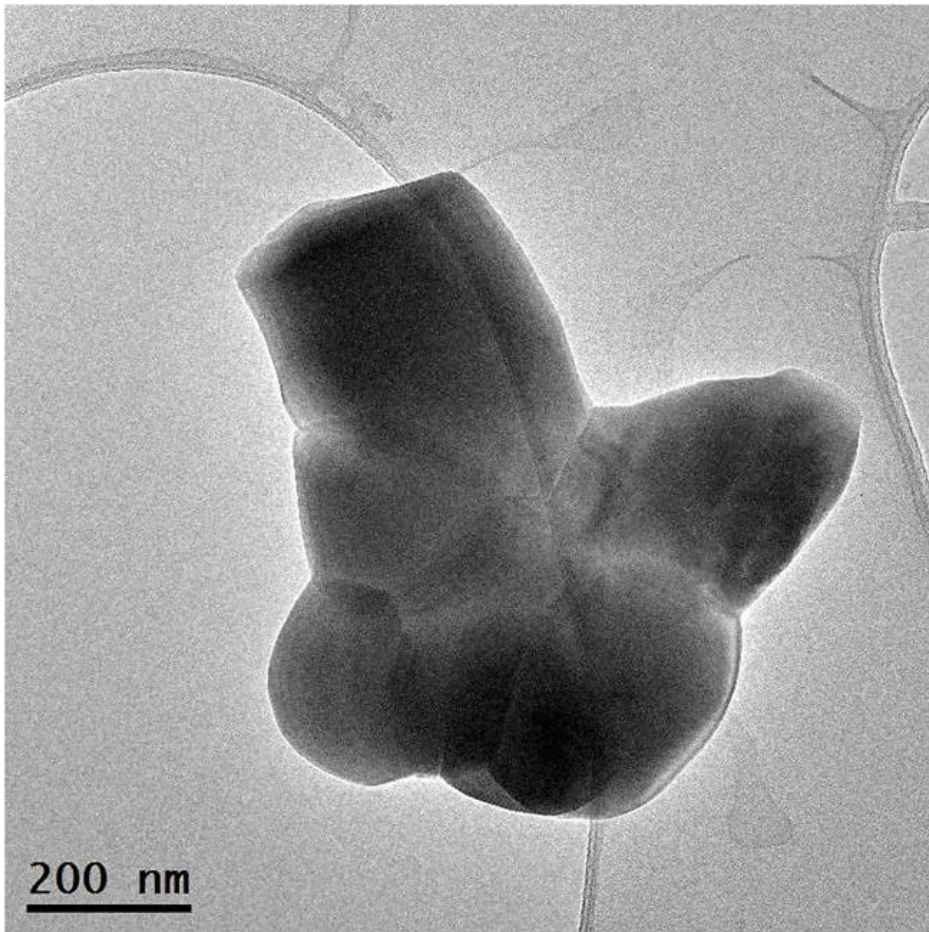


Figure S9. TEM image of PP/HAp(a) showing the sintering of the particles, which is caused by the applied thermal stimulated polarization treatment.